



ORIGINAL ARTICLE

Thermal, chemical, and structural investigation of the usability of Cs/nHAp-ZnO/Glutaraldehyde polymer matrix composite in potential biomaterial applications



Oktay Yigit

Faculty of Technology, Metallurgy and Material Engineering, Firat University, Elazığ, TURKEY

Received 3 January 2023; accepted 19 March 2023

Available online 23 March 2023

KEYWORDS

Chitosan;
Hydroxyapatite;
ZnO;
Polymeric Composites;
Cross-linking reaction

Abstract Nano-HAp and ZnO-containing particles in the main chitosan matrix that can be used as a scaffold composite or surface coating in dental and medical implants to improve infection and biocompatibility processes have been developed. After adding chitosan/HAp-ZnO biopolymer, a cross-linked triple absorbent composite system was produced using glutaraldehyde simply and practically. Morphological analyzes were examined by FE-SEM analysis, and the changes that occurred with the cross-linking reaction were observed. Elemental analysis of composite materials was analyzed with EDS, and chemical analyzes were analyzed using ART-IR, XPS XRD and Raman analysis. In addition, the thermal properties of the composites were examined by DTA and TGA analysis. As a result of the cross-linking reaction, it was observed that the composite exhibited a more compact structure. The study's primary purpose was to observe the ability of the biodegradable chitosan polymer to form composites with ZnO and HAp structure and examine the changes that occur with the cross-linking reaction. As a result, it was seen that the three components were well distributed among each other, intramolecular and intermolecular bonds were formed between these components, and the composite was restructured with the occurrence of strong interaction.

© 2023 The Author(s). Published by Elsevier B.V. on behalf of King Saud University. This is an open access article under the CC BY-NC-ND license (<http://creativecommons.org/licenses/by-nc-nd/4.0/>).

1. Introduction

Biomedical studies are now on the fabrication of nano-based composites and their various applications. Nano-composites are used in many applications, such as materials to improve the tissue healing process to be used in injuries (Diez-Pascual and Diez-Vicente, 2015), biomedical applications used in bone tissue engineering (Mallakpour and Okhovat, 2021) and coatings on metallic materials for dental and biomedical applications (Yigit et al., 2022, 2020). Among these developments, composite structures' most sought-after properties are

Peer review under responsibility of King Saud University.



improved biological, mechanical, and chemical properties. One of the biggest problems encountered in implants and tissue engineering is the insufficient biocompatibility of materials and bacterial infections. Various nano-composites are being developed to overcome these problems. Pereira et al. (2019), designed chitosan (Cs), polyethylene glycol, and hydroxyapatite (HAp) composite using different percentages of ZnO and CuO nanoparticles and investigated their bioactivity and antibacterial properties. In composites containing wt. 1% CuO and ZnO, HAp added composites showed the best antibacterial and bioactivity properties (Pereira et al., 2019). Murali et al. (2019), designed Ag/ZnO nanoparticles, Cs, and gelatin polymer composites by solution casting method. As a result, the mechanical properties and antibacterial activities of the Ag/ZnO additive were slightly improved (Murali et al., 2019).

Cs is a natural cationic polysaccharide with unique biological properties that exhibit superior biological properties, such as biodegradability, antigenicity, non-toxicity, and good biocompatibility (Chen et al., 2009; Cicek Ozkan, 2022; Cicek Ozkan et al., 2018). However, pure Cs has little or no antibacterial activity (Thomas et al., 2019). To improve the antibacterial activity of this polymer structure and increase its mechanical properties, some metals or metal oxides with antibacterial activity should be included in the composite (Sani et al., 2019). These additives are generally used as nanoparticles such as Ag, Cu, and ZnO, and besides exhibiting very high antibacterial properties compared to other reinforcement elements, their costs are relatively low (Rong et al., 2019). It is also possible to prevent antibiotic resistance in skin infections with composites prepared with these metallic nanoparticle supplements.

Recent studies have investigated the effects of ZnO doping on the antibacterial activity of natural polysaccharides in ZnO-doped composites. Tantiwatcharothai et al. (2019), used Basil seed mucilage with glycerol and ZnO and prepared a plasticized hydrogel mucilage-ZnO composite. The prepared composites exhibited excellent antibacterial activity against *Staphylococcus aureus* (*S. aureus*) and *Escherichia coli* (*E. coli*) (Tantiwatcharothai and Prachayawarakorn, 2019). Hezma et al. (2019), designed composites are containing Cs and PVA with different ratios of ZnO as nano-reinforcement elements. According to the results they obtained, it was reported that the amorphous phase, thermal stability, and antibacterial activity of the composite structure increased with the increase in the amount of ZnO additives (Hezma et al., 2019).

Bone tissue in the human body is a natural composite structure consisting of 65–70% hydroxyapatite (HAp) phase as the matrix and the other part organic phase (collagen, glycoproteins, proteoglycans, sialoproteins, etc.) (Cordonnier et al., 2011). HAp in bone is a hard tissue with ions (e.g., Na^+ , Mg^{2+} , Sr^{2+} , Mg^{2+} , Zn^{2+} , K^+ , CO_3^{2-}), which are very important for the body in terms of physicochemical and biological properties (Ratha et al., 2021). For this reason, synthetic HAp has been produced to replace the natural HAp structure in tissue engineering and has been able to successfully bio-mimic natural bone tissue (Fernandez-Yague et al., 2015).

However, prepared synthetic apatite structures lack ionic substituents and other organic structures, which are very important in natural bone structure. The need for doping and characterizing these substitutions has emerged. Many studies have focused on the synthesis and characterization of HAp doped with various additives as a bioactive phase that can be used for dental and bone regeneration (Ressler et al., 2021). Another type of study is HAp coating to produce biocomposites by adding synthetic HAp into composite structures or to improve the biological properties of metallic implants (Yigit et al., 2022, 2020). Studies on imitating organic phases of bone tissue have also gained momentum. Thus, natural bone tissue can be imitated. Natural polymers (for example, collagen, gelatin, chitosan, glycosaminoglycans, and silk fibrin) are frequently used in various tissue engineering studies and subsequently in various applications (Ressler et al., 2022b). Since these polymers are natural structural elements of biological tissues, they exhibit excellent biological properties and show

superior osteointegration without damaging cells (Ressler et al., 2021). Chitosan (Cs), a natural amino polysaccharide used in many studies, finds the most use with HAp in polymer-based studies. Composed of randomly distributed β -(1–4)-linked d-glucosamine (glucosamine) and N-acetyl-d-glucosamine (N-acetylglucosamine) building units, this polymer is similar to glycosaminoglycan found in natural bone tissue. And modulates the bioavailability and activity of various osteoclastic and osteogenic factors at the cellular level (Islam et al., 2017; Mansouri et al., 2017; Ressler et al., 2022b; Tan et al., 2009). Therefore, Chitosan and hydroxyapatite nanocomposites (Cs/nHAp) have been highly sought as potential scaffolds for bone tissue engineering (BTE) applications. In addition, Cs/HAp scaffolds can be used for bone regeneration in bone defects placed in parts of native bone tissue that are not exposed to mechanical stress and loads (Fernandez-Yague et al., 2015; Levensgood and Zhang, 2014). The most crucial challenge in bone tissue applications is to produce structures with suitable surface properties and mechanical strength to allow cell proliferation, growth, proliferation, adhesion, and differentiation (Fernandez-Yague et al., 2015; Roseti et al., 2017). In addition, Cs/nHAp composite structures support biological properties and bioactivity (Ressler et al., 2022a).

This study will prepare composites by doping nano-HAp and ZnO into chitosan (Cs) polymer. The first of the composites to be prepared will be prepared without adding glutaraldehyde as a crosslinker, and the other composite will be cross-linked by adding glutaraldehyde to chitosan. The formation of polymer structure with ZnO and nano-HAp additives will be examined, and the ability to form composites with ZnO and nano-HAp additives doped as a result of cross-linking reaction will be examined. The composites to be obtained will be essential for biomedical applications, bone tissue engineering, dental studies, implant coatings, and medical applications used in wound healing processes.

2. Materials and methods

2.1. Materials

Low molecular weight Cs ($\text{C}_{56}\text{H}_{103}\text{N}_9\text{O}_{39}$, 1526.5 g/mol molecular weight and 75–80% Deacetylated chitin, Poly(D-glucosamine) and ZnO (Purity: 99.9%, Size: 3 nm) were purchased from Sigma-Aldrich. nHAp (nano-XIM phase purity 100, size < 50 nm) was purchased from FLUIDINOVA, and glutaraldehyde ($\text{C}_4\text{H}_8\text{O}_4$ crystalline) and acetic acid ($\text{CH}_3\text{CO}_2\text{H}$, $\geq 99\%$ assay) were purchased from Sigma-Aldrich.

2.2. Preparation of Cs/nHAp-ZnO composites

Composites were prepared using two different methods, First, a ZnO-nHAp hybrid was prepared. For this, 25 mg of ZnO and 1 g of aqueous nano-HAp (wt. 30%) were mixed in a magnetic stirrer for 2 h in a 100 mL deionized water. It was then left to dry for 6 h at 60 °C. Two different composites were produced with the prepared hybrid mixture. Composites will be described as A and B.

A – Cs/nHAp-ZnO: Chitosan prepared with vol. 5% acetic acid solution was mixed with vol. 50% hybrid ZnO-HAp and stirred with a magnetic stirrer for 24 h at room conditions. It was dried with stirring until the acid was removed.

B- Cs/nHAp-ZnO/GIA: Chitosan prepared with vol. 5% acetic acid solution was mixed with vol. 50% hybrid ZnO-HAp in a 40 mL deionized water at room conditions. 0.5 mL of vol. 10% glutaraldehyde was added to the mixture. It was dried by stirring for 24 h.

Atomic bonding models of Chitosan, ZnO, nHAp, and glutaraldehyde structures used in the preparation of composites are given in Fig. 1.

2.3. Characterizations

The prepared composites are polymer-based in the form of large sheets. Therefore, it was not required to be prepared in a special form for each analysis. Therefore, the prepared polymer-based composites were directly characterized by shearing in millimeters.

To confirm the composition of Cs/nHAp-ZnO and Cs/nHAp-ZnO/GIA composites was analyzed using a Grazing incidence X-ray diffraction (GI-XRD) (PANalytical Empyrean, London, UK) system using monochromatic Cu-K α radi-

ation ($\lambda = 0.15406$ nm). XRD results were defined using X'Pert Highscore plus software.

Attenuated total reflection infrared (ATR-IR) spectroscopy was used to examine the functional groups of Cs/nHAp-ZnO-based composites using the Thermo Scientific Nicolet iS 5 FT-IR Spectrometer (Nicolet Instrument Corporation, Madison, WI). The ATR-IR spectra of the coatings were recorded on an FTIR spectrometer with a single reflection horizontal ATR accessory. Scans were performed in the range of 500–4000 cm^{-1} and with a spectral resolution of 0.5 cm^{-1} .

Surface morphologies, the form of the chitosan matrix, elemental analysis of the composites, and the formation of nHAp and ZnO structures on the surface were investigated using a field emission scanning electron microscope (JSM-7001F, Jeol, Tokyo, JP) equipped with energy dispersive spectroscopy

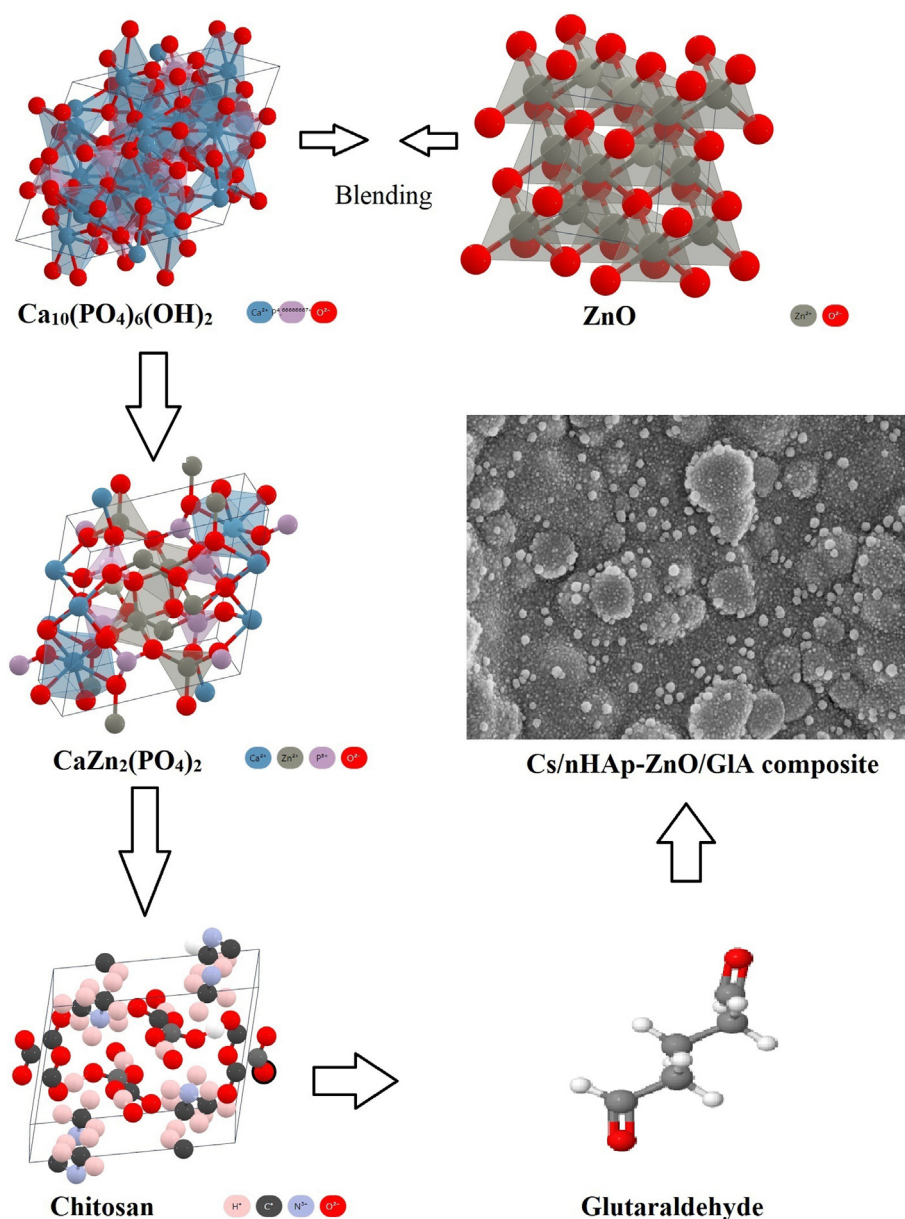


Fig. 1 Atomic bonding models of Chitosan, ZnO, HAp, and glutaraldehyde structures.

(EDS, Inca system) used with secondary electrons below 15 kV.

The basic chemical composition of the composites and their chemical bonds were investigated using X-ray photoelectron spectra (XPS) on the Specs-Flex XPS system (SPECS Surface Nano Analysis GmbH, Zurich, DE). Photoemission was induced using monochromatic Al K α radiation (1486.6 eV). Before XPS analysis, composite materials were etched with a 1 min Ar⁺ ion bombardment to remove contamination. The beam spot size is approximately 200 μ m. Peak deconvolution and background subtraction were performed with the CasaXPS and Origin programs.

TG/DTA (Shimadzu TA-60 WS, Kyoto, JP) measurements were made at a heating rate of 10 $^{\circ}$ C/min from room temperature to 600 $^{\circ}$ C. TG/DTA measurements were performed for all composites in order to observe the thermal stability of the samples.

3. Results and discussions

3.1. XRD analyzes of Cs/nHAp-ZnO composites

In Fig. 2, the XRD graph of nHAp-ZnO and chitosan polymer matrix composite and glutaraldehyde added composite is given. The JCPDS cards for Cs is 00-039-1894, for HAp is 00-025-0166, for Parascholzite ($\text{CaZn}_2(\text{PO}_4)_2$) is 00-035-0495. The presence of HA-Zn and Chitosan peaks can be detected in the graphs of the composites. HAp peaks observed at $2\theta = 25,803^{\circ}$, $31,624^{\circ}$ and $32,778^{\circ}$. Parascholzite is a calcium zinc phosphate compound and in XRD peaks at $2\theta = 10,388^{\circ}$, $19,351^{\circ}$, $21,351^{\circ}$ and $31,890^{\circ}$ shows that the interaction of this compound. Chitosan shows its characteristic peak at $2\theta = 19-20^{\circ}$ [9]. With the addition of glutaraldehyde, this amorphous peak was suppressed, and a more crystalline polymer composite was formed. In addition, the peaks of nHAp and ZnO, which remained at low intensity in the amorphous polymer, became more pronounced. As a result, peaks of the Parascholzite and HAp with higher intensity are observed in the structure formed by the cross-linking reaction. It also shows that nHAp-ZnO and chitosan molecular interactions occur with the addition of glutaraldehyde in the chitosan com-

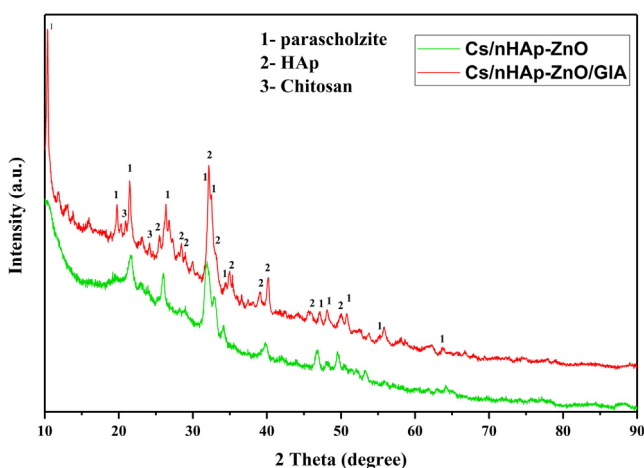


Fig. 2 XRD graphs of the Cs/nHAp-ZnO and Cs/nHAp-ZnO/Glutaraldehyde composites.

posite (Istifarah, 2012; Nikpour et al., 2012; Wicaksono et al., 2017). The emergence of parascholzite compound due to the interaction of ZnO and nHAp in the structure was observed after the cross-linking reaction. This is because the compounds with high crystalline structure in the amorphous Cs structure remained at low intensities. Still, the cross-linked Cs polymer structure with the addition of glutaraldehyde transformed from an amorphous structure to an amorphous-crystalline structure, allowing higher intensity peaks to be read than other compounds.

3.2. ATR-IR analyzes of Cs/nHAp-ZnO-based composites

ATR-IR analyzes are shown in Fig. 3. Functional groups of Cs/nHAp-ZnO-based composites were investigated by ATR-IR analysis. When the chitosan matrix composites are examined, the change in peak intensities with the addition of glutaraldehyde draws attention. In other words, after the cross-linking reaction, the crystallinity of chitosan matrix nHAp-ZnO added composites changes, and their spectral models differ from glutaraldehyde-free chitosan composites. However, major functional groups are present in both composites. In the range of approximately 3400–3700 cm^{-1} , OH⁻ peaks are observed depending on the stretching vibration band of the water. Chitosan is defined with N–H peaks at approximately 1600 cm^{-1} . In addition, C–H vibrational bands in the range of 2840–3333 cm^{-1} belong to the chitosan structure. In addition to chitosan, for nHAp, when the composite structure is examined, PO_4^{3-} turning mode occurs as a bicentric ν_1 mode peak at 834 cm^{-1} and 1184 cm^{-1} , respectively. Symmetrical stretching (ν_3) is observed at 988 cm^{-1} , and asymmetric stretching mode (ν_2) is observed at 1133 and 916 cm^{-1} . In addition, one pair with a peak of 618 cm^{-1} and the other of 561 cm^{-1} is attributed to the bending vibration (ν_4) of PO_4^{3-} (Gao et al., 2015). PO_4^{3-} asymmetrical turn bands are seen at 1155, 588, and 561 cm^{-1} (Feng et al., 2016; Nosrati et al., 2019). The band seen at 790 cm^{-1} is attributed to the release mode of the hydroxyl group. In addition, with the addition of glutaraldehyde, the intensity of the OH⁻ peak in the 3400 cm^{-1} range and the C–H peak in the 2800–3333 cm^{-1} range of the composite decreased. Also, the amide peak

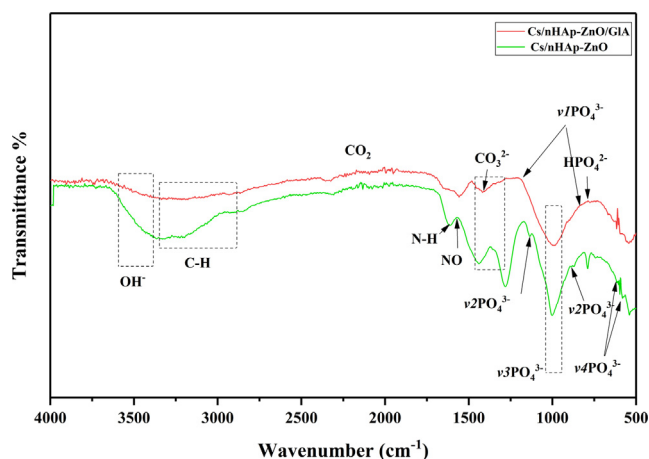


Fig. 3 ATR-IR spectra of the Cs/nHAp-ZnO and Cs/nHAp-ZnO/Glutaraldehyde composites.

around 1600 cm^{-1} showed similar behavior. In the range of $2100\text{--}2226\text{ cm}^{-1}$, the CO_2 vibration band is seen passing through the atmosphere, and in the range of $1272\text{--}1414\text{ cm}^{-1}$, it depends on the vibration of the CO_3^{2-} group. These results were compatible with the obtained XRD data. They proved that the synthesis of Cs/nHAp-ZnO composite and glutaraldehyde added composite produced by the cross-linking reaction of the same composite by blending method was successful. The decreasing intensity and broadening of the peaks indicate interactions between the elements that make up the composite, such as the hydrogen bond between chitosan and hydroxyapatite (Díez-Pascual and Díez-Vicente, 2015; Rahman et al., 2020; Warastuti et al., 2018). Thus, it proves that the ability of chitosan, nHAp, and ZnO compounds to form composites is successful.

3.3. Raman spectra of Cs/nHAp-ZnO and Cs/nHAp-ZnO/Glutaraldehyde composites

Fig. 4 shows the Raman spectra of Chitosan, nHAp, and zinc oxide composites. In the case of visible region excitation, Raman bands in chitosan/nHAp-ZnO composite without glutaraldehyde are exhibited at a lower rate compared to glutaraldehyde-added composites with the Raman spectrum. Prominent bands at 326.6 , 432.6 , and 570 cm^{-1} confirm the presence of ZnO in the composite. The main band observed for ZnO at 432.6 cm^{-1} can be correlated with the non-polar optical phonon E2 (high) mode in ZnO. Also, two frequencies belong to non-polar phonon modes with E2 symmetry. These are the phonon modes associated with E2 (high) oxygen atoms and the other associated with E2 (low) Zn-sublattice (Abiraman et al., 2016; Panda et al., 2014). The most important reason for the shift in wave numbers and the change in band shapes in the Raman spectrum is the interaction between ZnO and nHAp and its strong distribution into the chitosan matrix. This interaction increased significantly due to the cross-linking reaction, and the recorded Raman spectra showed that the interaction of ZnO and nHAp increased with cross-linking in the chitosan matrix. It shows the presence of a parascholzite structure with good crystal quality in good

agreement with the XRD analysis. Analysis by Raman spectroscopy of chitosan matrix composite containing nano-hydroxyapatite and ZnO also prove the presence of hydroxyapatite and chitosan in the prepared composite. A high band characterizes the Raman spectrum of chitosan at 1070 cm^{-1} attributed to stretching vibrations $\nu(\text{O}=\text{S}=\text{O})$. The Raman spectrum of hydroxyapatite is characterized by a high band of 960 cm^{-1} assigned to the symmetric $\nu\text{P-OH}$ stretching vibration, while $\delta\text{PO-H}$ bending and $\nu\text{asP-OH}$ are asymmetrical as reported by other bands (1014 , 1099 , 1072 cm^{-1}) known as stretching vibrations. (Cukrowski et al., 2007). As mentioned earlier, a chitosan peak at 1068 cm^{-1} characterizes chitosan in the Raman spectrum, with a density difference in Cs/nHAp-ZnO composites reflecting the different proportions of chitosan in the samples. The high peak of hydroxyapatite at 960 cm^{-1} is seen in both glutaraldehyde-added and undoped composites, but the peak intensities vary. It is the transformation of the chitosan matrix from amorphous to a more crystalline structure after the cross-linking reaction so that the peak intensities obtained from nano-structured HAp are read differently.

Raman spectra of glutaraldehyde added and undoped composites are different in Cs/nHAp-ZnO composite structures. After cross-linking reaction with glutaraldehyde additive, the Raman spectrum (Fig. 4) shows characteristic peaks of ZnO, hydroxyapatite, and chitosan at 432 cm^{-1} , 960 cm^{-1} , and 1070 cm^{-1} , respectively. The peaks give different densities for the two different composites. In addition, the intense peak at 2885 cm^{-1} corresponds to the $\nu(\text{CH}_2)$ stretching vibrations, and the intense peak at 1654 cm^{-1} corresponds to the $\nu(\text{CO})$ vibration peak. The peaks at 1437 and 1550 cm^{-1} are associated with amide groups and are attributed to asymmetric vibration $\delta\text{as}(\text{CH}_3, \text{CH}_2)$ and asymmetric vibration $\delta(\text{NH}_2)$ bands, respectively (Escobar-Sierra et al., 2015). When the Raman spectrum and ATR-IR analyzes are compared, it is seen that they give very consistent results. In addition, the obtained Raman spectrum shows that the composite structures were created successfully.

3.4. XPS spectrum of the Cs/nHAp-ZnO and Cs/nHAp-ZnO/GIA composites

General and elemental analyses of Cs/nHAp-ZnO and Cs/nHAp-ZnO/GIA composites were performed with XPS. General XPS scan results are given in Fig. 5, and atomic ratios are given in Table 1. In the general scan, all the elements in the composite structure were detected, and then the analysis was completed by making high-resolution scans. In Fig. 6, high-resolution XPS spectra are given.

The high-resolution XPS spectrum clearly shows the presence of only Zn, C, O, N, Ca, and P in the Cs/nHAp-ZnO and Cs/nHAp-ZnO/GIA composites. The core level peak detection spectrum for Zn^{2+} gives the main peaks at 1021.34 and 1044.26 eV , corresponding to the Zn 2p_{3/2} and 2p_{1/2} core levels. The eV values of 283.9 , 285.23 , 287.49 , and 289.31 for the glutaraldehyde-free Cs/nHAp composite correspond to (C-H-N), (C-H-N), (O = C-O/C = O) and (H-C-O/O-H), respectively. In the Cs/nHAp-ZnO/GIA composite, the peaks at 284.1 , 285.01 , 286.12 , and 288.33 eV are (C-C/C-H), (C-H-N), (O-C-O) and (O = C-H/C = O) binding respectively. Examining the O 1s spectrum, (Zn-O), (C-OH), and (C-O)

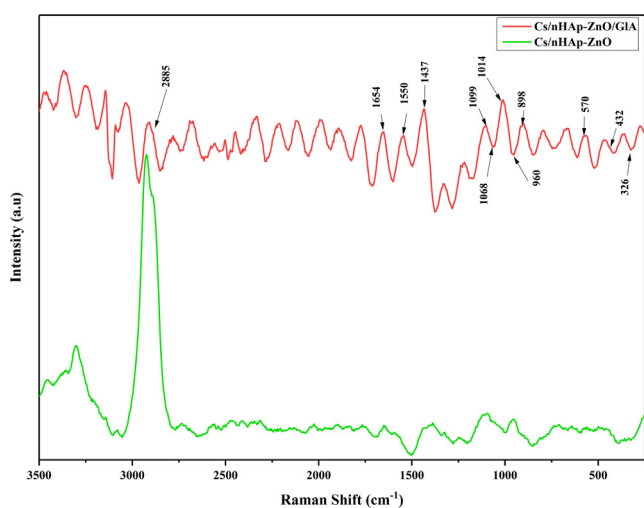


Fig. 4 Raman spectra of Cs/nHAp-ZnO and Cs/nHAp-ZnO/Glutaraldehyde composites.

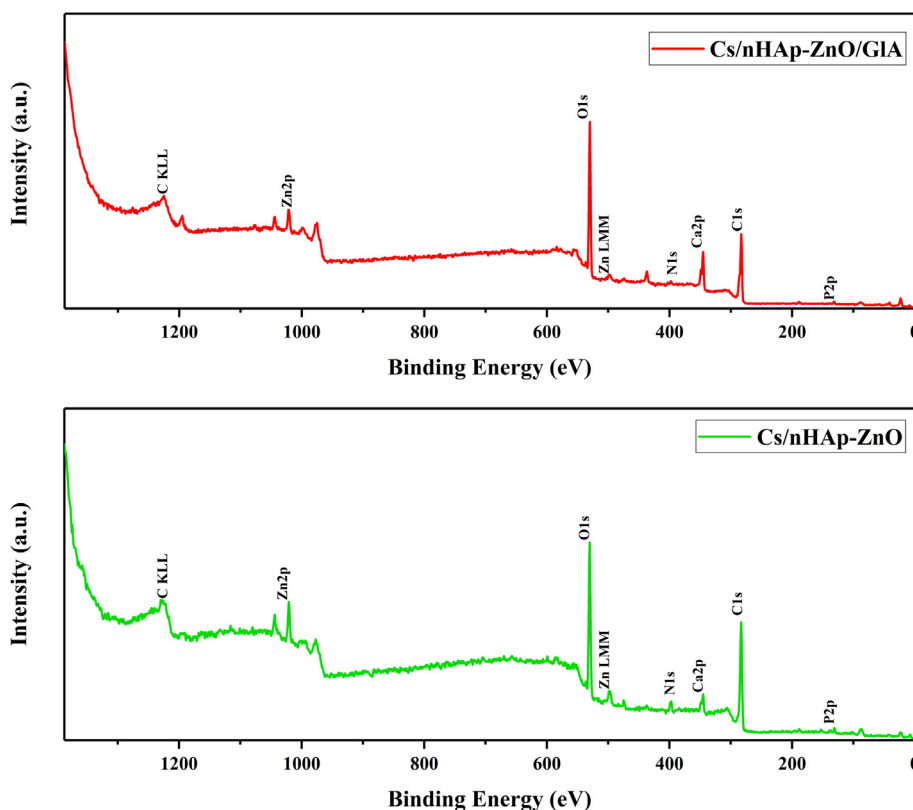


Fig. 5 The wide survey XPS spectra of Chitosan/nHAp-ZnO and Chitosan/nHAp-ZnO/GIA composites.

Table 1 Atomic ratio of the elements in Chitosan/nHAp-ZnO and Chitosan/nHAp-ZnO/GIA composites from the wide survey XPS spectra.

	Name	Position	Atomic%
Cs/nHAp-ZnO	O 1 s	531.5	25,09
	C 1 s	284.5	67,76
	N 1 s	398.5	2,46
	Ca 2p	346.5	2,54
	Zn 2p 3/2	1022.5	1,62
	P 2p	132.5	0,53
	Cs/nHAp-ZnO/GIA	O 1 s	531.5
C 1 s		284.5	59,35
N 1 s		399.5	1,16
Ca 2p		346.5	6,33
Zn 2p 3/2		1022.5	0,52
P 2p		132.5	1,36

have binding energies of 531.8, 532.47, and 534.27 eV. Corresponding to (C–H–N) at 393.43 eV, (N–ZnO) at 399.23 eV, (N–O–H) at 399.8 eV, and (C–N) at 401.72 eV N 1 s peak values were also observed. When Ca 2p_{3/2} peaks are examined, peaks corresponding to the Ca 2p_{3/2} core level at 346.99 eV and peaks corresponding to the Ca 2p_{1/2} core level at 350.58 eV are seen. The main peak of the P 2p core level occurred at 135.29 eV. When examining the XPS spectrum, ZnO and nHAp structures are strongly adorned by chitosan. XPS spectrum of glutaraldehyde added and undoped compos-

ites in Zn and nHAp doped chitosan composites prove the presence of zinc ions, Ca, and P ions. The results obtained are consistent with the XRD and Raman results. In addition, the addition of Glutaraldehyde changed the binding energies, albeit in a small amount. This proves that a change in the composite structure occurs with the cross-linking reaction in the obtained composite structure. The results of this research study are consistent with literature reports (Abiraman et al., 2016; Lin et al., 2021; Sarma et al., 2020).

3.5. SEM images of the Chitosan/nHAp-ZnO and Chitosan/nHAp-ZnO/GIA composites

The morphologies of two different composites prepared by incorporating nHAp and ZnO into chitosan and cross-linked with glutaraldehyde were examined using FESEM at 1000x, 2500x, and 5000x magnifications (Fig. 7). In Fig. 8 25000x and 50000x FESEM images are given. FESEM images of the Cs/nHAp-ZnO composite (Fig. 7(a)) show that chitosan exhibits a sheet-like morphology. In addition, the general surface morphology of the composite structure does not exhibit an utterly homogeneous distribution, and chitosan fibers can be seen on the surface. It is observed that the homogenization of the surfaces increased, and more crystalline structures were formed in some regions in the cross-linked chitosan composite with glutaraldehyde doped at lower magnifications (Fig. 7(b)). It can be understood that ZnO and nHAp layers are visible on the composite surface in the high-magnification FESEM images given in Fig. 8(a). In addition, the irregularity of the chitosan layers on the surface caused the dense formation of

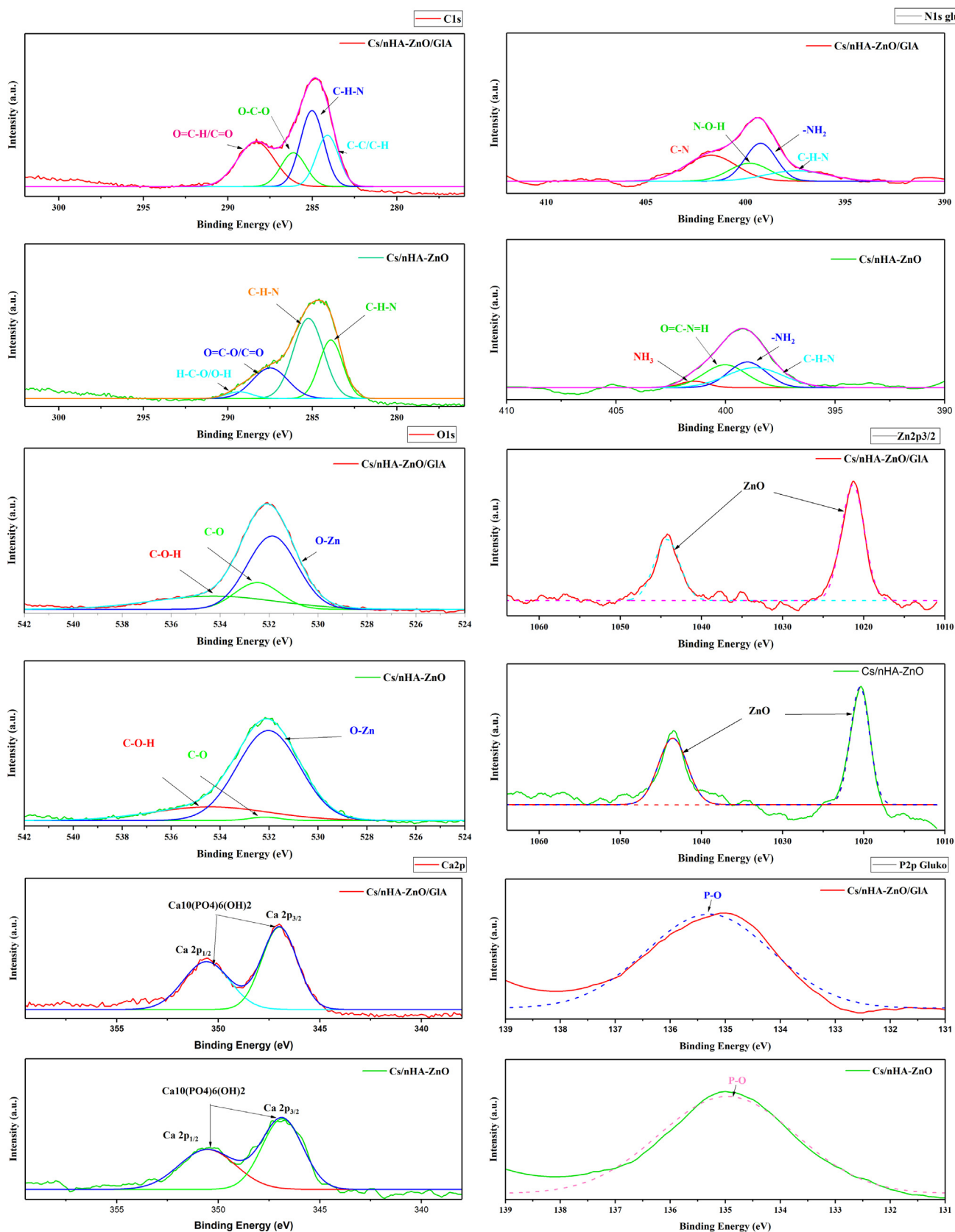


Fig. 6 High resolution XPS spectrum of C 1 s, N 1 s, Zn 2p_{3/2}, O 1 s, Ca 2p and P 2p.

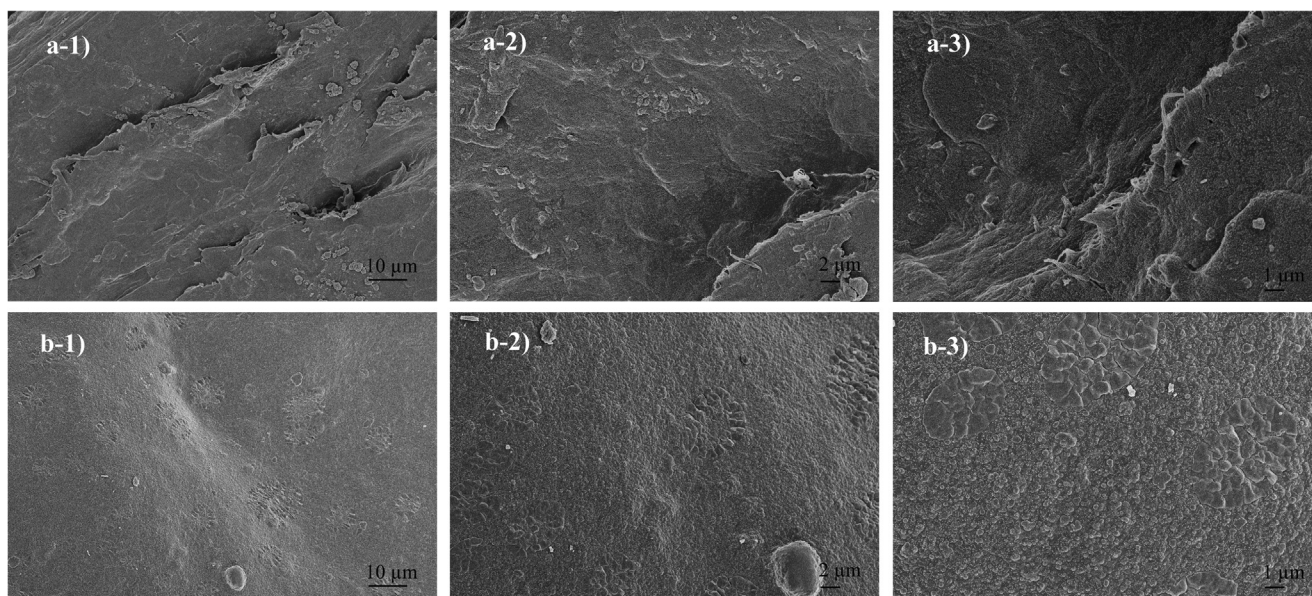


Fig. 7 SEM images of the composites a) 1000x, 2500x and 5000x magnification of Chitosan/nHAp-ZnO b) 1000x, 2500x and 5000x magnification of Chitosan/nHAp-ZnO/GIA.

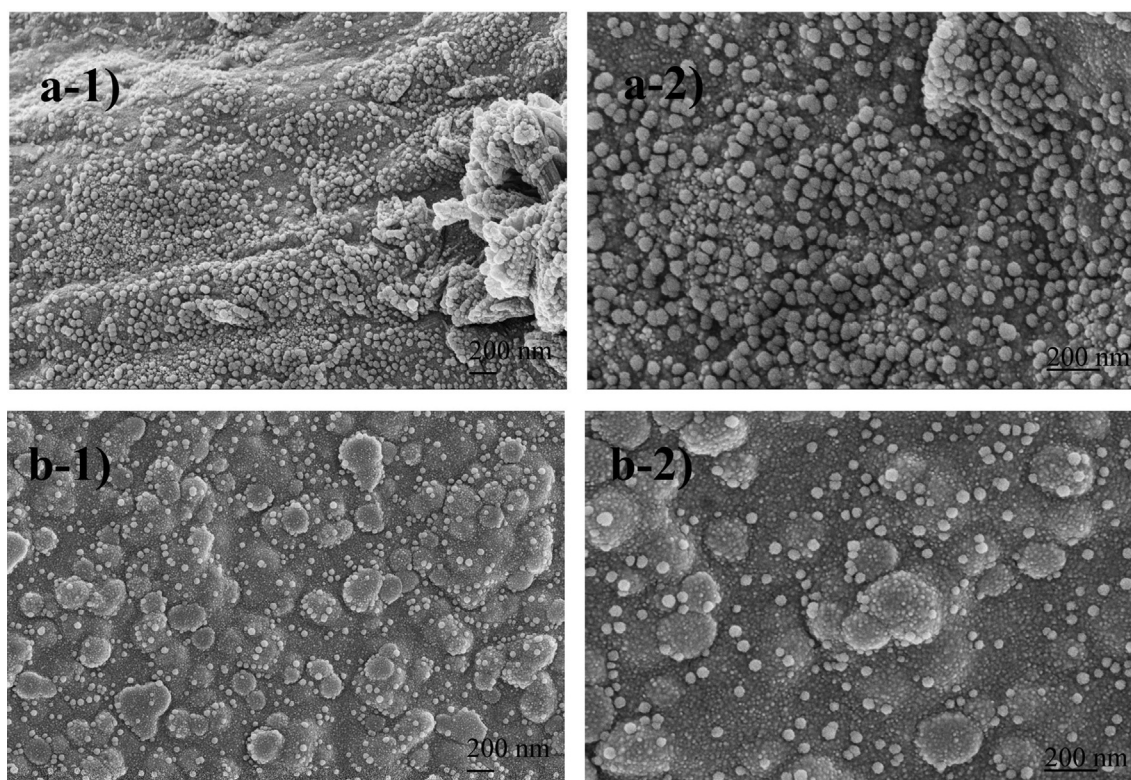


Fig. 8 SEM images of the composites a) 25000x and 50000x magnification of Chitosan/nHAp-ZnO b) 25000x and 50000x magnification of Chitosan/nHAp-ZnO/GIA.

ZnO and nHAp particles in these regions. Composite surface morphology exhibits a distinctive structure in the form of large agglomerations. When the morphology of the glutaraldehyde-added composite is examined (Fig. 8(b)), it can be said that the composite surface forms a formation with finer grains and

smaller particles. ZnO and nHAp particles showed better binding into the chitosan matrix. ZnO and nHAp particles formed as spherical aggregates in the chitosan matrix. Based on the above results, it can be said that chitosan composites with cross-linking reaction with glutaraldehyde add a more uniform

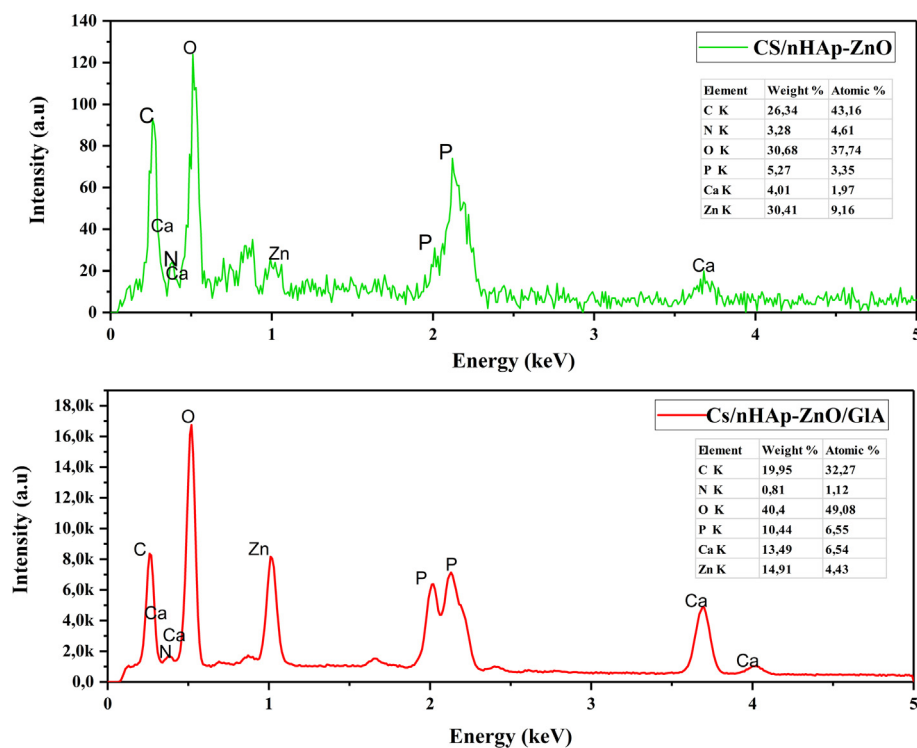


Fig. 9 EDS spectra of Chitosan/nHAp-ZnO and Chitosan/nHAp-ZnO/GIA composites.

and smooth morphology in ZnO and nHAp-doped chitosan composites than chitosan composites without cross-linking reaction (Rahman et al., 2020).

3.6. EDS spectra of the Chitosan/nHAp-ZnO and Chitosan/nHAp-ZnO/GIA composites

EDS analyses of Cs/nHAp-ZnO and Cs/nHAp-ZnO/GIA composites are given in Fig. 9, respectively. When the EDS analyzes were examined, C, O, N, Zn, Ca, and P elements expected to be seen in the composite structure were observed, and no impurities were found. Furthermore, the Ca and P ratios of the chitosan composite with glutaraldehyde added significantly increased compared to the undoped composite. On the other hand, there is a slight decrease in the Zn ratio. This is because the composite structure exhibits a more homogeneous structure with the glutaraldehyde additive and chitosan successfully forms composites with all additives. Accordingly, the peak intensity read from all elements gave a very high value, and it is thought that the composite structure exhibits a more crystalline structure. Previous XRD, ATR-IR, Raman, and SEM analyses also support this idea.

3.7. TGA and DTA analyzes of the Cs/nHAp-ZnO and Cs/nHAp-ZnO/GIA composites

Thermal stability in biomaterials can be considered an essential property due to the need for sterilization for whatever purpose it is used. For this reason, the degradation and thermal behavior of polymer-based biomaterials against thermal processes is a characterization that needs to be examined. Therefore, the TGA of Cs/nHAp-ZnO and Cs/nHAp-ZnO/GIA

biocomposites were evaluated from room temperature to 600 °C. TGA graphics are presented in Fig. 10, and DTA graphics are presented in Fig. 11. In the temperature range studied, chitosan was decomposed entirely and characterized by a three-degradation profile; The initial weight loss occurs due to the removal of water from the composite structure at temperatures up to 120 °C. The second weight loss is defined as cleavage of branched-chain structures, depolymerization of chitosan, and dehydration of its molecular chains, which appear between 210 and 250 °C. The final weight loss is due to the oxidative decomposition of the carbon-based residue produced in the second thermal event, which appears between 450 and 580 °C [40].

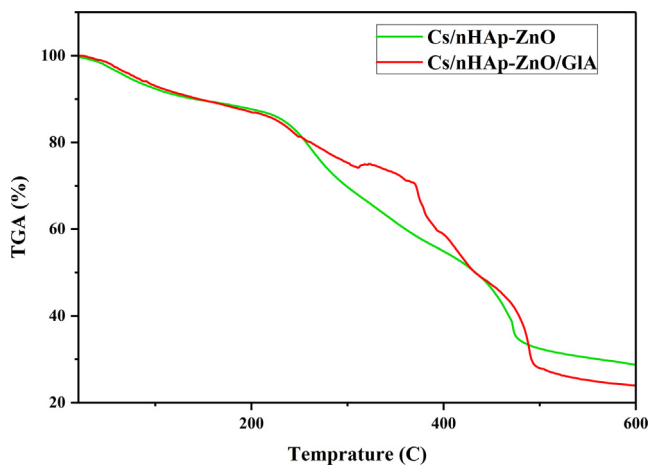


Fig. 10 Thermogravimetric analysis (TGA) of the Cs/nHAp-ZnO and Cs/nHAp-ZnO/GIA composites.

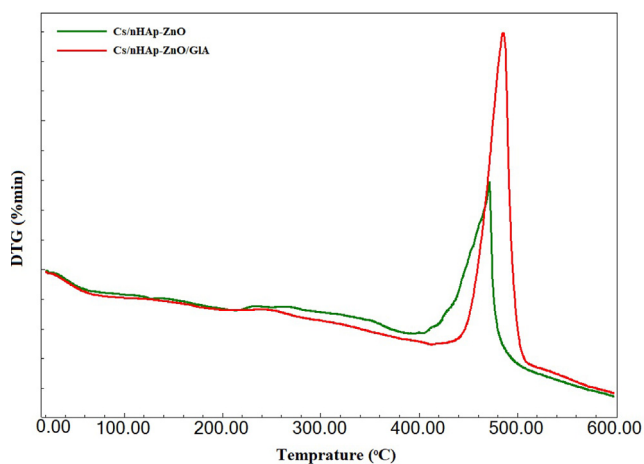


Fig. 11 DTA analyzes of Cs/nHAp-ZnO and Cs/nHAp-ZnO/GIA composites.

The nHAp structure contains two types of water: adsorbed water and caged water. The adsorbed water does not show any effect on the cage parameters. It is removed from the structure reversibly from room temperature to 200 °C. However, cage water is irreversibly lost from the structure in the temperature range of about 250–450 °C and appears as a shrinkage of cage dimensions during heating. When the two composite structures were compared, they formed a similar curve from room temperature to 200 °C. However, the chitosan composite produced by the cross-linking reaction showed a lower degradation rate than the glutaraldehyde-free composite. Glutaraldehyde-added chitosan composite exhibits a more stable structure in this temperature range where polymer chains are thermally degraded; that is, it maintains its thermal stability more. After 450 °C, both composites degraded irreversibly, and no significant weight loss was observed after 550 °C.

4. Conclusions

This study synthesized chitosan matrix nHAp and ZnO doped biopolymer composites. Chitosan was more evenly distributed between the composites formed by adding nHAp-ZnO in the matrix and nHAp and ZnO particles, resulting in better bonding. At the next stage, the composite structure exhibited a more uniform and homogeneous structure with the glutaraldehyde added into the Chitosan/nHA-ZnO composite. The ZnO and nHAp structures were better adapted within the structure after the cross-linking reaction. Particles more prominent on the glutaraldehyde-free composite surface were dispersed into the structure and transformed from a layered and fibrous composite structure to a more dense and smooth structure. In addition, chitosan, a natural biopolymer with nHAp and ZnO structures, can exhibit high biocompatibility and bioactivity. XRD, ATR-IR, and XPS analyzes showed that all standard components appeared in the composite structure. It has been observed that the components obtained in the composite can preserve their main properties without deterioration and pass with good adaptation within the structure. Thermal gravimetric analysis showed that the composite structure's thermal resistance increased with the addition of glutaraldehyde. The presented study proved that both composites prepared with chitosan, nHAp, and ZnO and then formed by cross-linking reaction with the addition of glutaraldehyde could form composites successfully. In addition, a more crystalline and thermally stable composite structure can be produced with the cross-linking reaction. Cross-linked composite with chi-

tosan matrix and containing nHAp and ZnO has a high potential for use as a coating and filling element in implant materials or as a scaffold.

Declaration of Competing Interest

The authors declare that they have no known competing financial interests or personal relationships that could have appeared to influence the work reported in this paper.

Acknowledgements

Thanks, Betül ÇİÇEK ÖZKAN, and Melek GÜNER, for their help and knowledge support in the study. This research did not receive any specific grant from funding agencies in the public, commercial, or not-for-profit sectors.

References

- Abiraman, T., Kavitha, G., Rengasamy, R., Balasubramanian, S., 2016. Antifouling behavior of chitosan adorned zinc oxide nanorods. *RSC Adv.* <https://doi.org/10.1039/c6ra13321e>.
- Chen, H. Te, Hsiao, C.H., Long, H.Y., Chung, C.J., Tang, C.H., Chen, K.C., He, J.L., 2009. Micro-arc oxidation of β -titanium alloy: Structural characterization and osteoblast compatibility. *Surf. Coatings Technol.* <https://doi.org/10.1016/j.surfcoat.2009.06.043>.
- Cicek Ozkan, B., 2022. Cellulose and chitosan biopolymer composites reinforced with graphene and their adsorption properties for basic blue 41. *Cellulose* 29, 9637–9655. <https://doi.org/10.1007/s10570-022-04852-8>.
- Cicek Ozkan, B., Soganci, T., Turhan, H., Ak, M., 2018. Investigation of rGO and chitosan effects on optical and electrical properties of the conductive polymers for advanced applications. <https://doi.org/10.1016/j.electacta.2018.11.032>
- Cordonnier, T., Sohier, J., Rosset, P., Layrolle, P., 2011. Biomimetic materials for bone tissue engineering - state of the art and future trends. *Adv. Eng. Mater.* <https://doi.org/10.1002/adem.201080098>.
- Cukrowski, I., Popović, L., Barnard, W., Paul, S.O., van Rooyen, P. H., Liles, D.C., 2007. Modeling and spectroscopic studies of bisphosphonate-bone interactions. The Raman, NMR and crystallographic investigations of Ca-HEDP complexes. *Bone.* <https://doi.org/10.1016/j.bone.2007.05.008>.
- Díez-Pascual, A.M., Díez-Vicente, A.L., 2015. Wound healing bio-nanocomposites based on castor oil polymeric films reinforced with chitosan-modified ZnO nanoparticles. *Biomacromolecules.* <https://doi.org/10.1021/acs.biomac.5b00447>.
- Escobar-Sierra, D.M., Martins, J., Ossa-Orozco, C.P., 2015. Chitosan/hydroxyapatite scaffolds for tissue engineering manufacturing method effect comparison. *Rev. Fac. Ing.* <https://doi.org/10.17533/udea.redin.n75a04>
- Feng, G., Cheng, X., Xie, D., Wang, K., Zhang, B., 2016. Fabrication and characterization of nano prism-like hydroxyapatite coating on porous titanium substrate by combined biomimetic-hydrothermal method. *Mater. Lett.* 163, 134–137. <https://doi.org/10.1016/j.matlet.2015.10.063>.
- Fernandez-Yague, M.A., Abbah, S.A., McNamara, L., Zeugolis, D.I., Pandit, A., Biggs, M.J., 2015. Biomimetic approaches in bone tissue engineering: Integrating biological and physicommechanical strategies. *Adv. Drug Deliv. Rev.* <https://doi.org/10.1016/j.addr.2014.09.005>.
- Gao, F., Xu, C., Hu, H., Wang, Q., Gao, Y., Chen, H., Guo, Q., Chen, D., Eder, D., 2015. Biomimetic synthesis and characterization of hydroxyapatite/graphene oxide hybrid coating on Mg alloy with enhanced corrosion resistance. *Mater. Lett.* <https://doi.org/10.1016/j.matlet.2014.09.088>.

- Hezma, A.M., Rajeh, A., Mannaa, M.A., 2019. An insight into the effect of zinc oxide nanoparticles on the structural, thermal, mechanical properties and antimicrobial activity of Cs/PVA composite. *Colloids Surfaces A Physicochem. Eng. Asp.* <https://doi.org/10.1016/j.colsurfa.2019.123821>.
- Islam, S., Bhuiyan, M.A.R., Islam, M.N., 2017. Chitin and chitosan: structure, properties and applications in biomedical engineering. *J. Polym. Environ.* <https://doi.org/10.1007/s10924-016-0865-5>.
- Istifarah, 2012. Sintesis dan Karakterisasi Komposit Hidroksiapatit dari Tulang Sotong (Sepia.sp)-Kitosan untuk Kandidat Bone Filler. *Skripsi Fak. Mat. dan Ilmu Pengetah. Alam. Jurnal Farmasi UIN Alauddin Makassar*, 2017, 5.1: 9-15.
- Levengood, S.K.L., Zhang, M., 2014. Chitosan-based scaffolds for bone tissue engineering. *J. Mater. Chem. B.* <https://doi.org/10.1039/c4tb00027g>.
- Lin, M.H., Wang, Y.H., Kuo, C.H., Ou, S.F., Huang, P.Z., Song, T. Y., Chen, Y.C., Chen, S.T., Wu, C.H., Hsueh, Y.H., Fan, F.Y., 2021. Hybrid ZnO/chitosan antimicrobial coatings with enhanced mechanical and bioactive properties for titanium implants. *Carbohydr. Polym.* <https://doi.org/10.1016/j.carbpol.2021.117639>.
- Mallakpour, S., Okhovat, M., 2021. Hydroxyapatite mineralization of chitosan-tragacanth blend/ZnO/Ag nanocomposite films with enhanced antibacterial activity. *Int. J. Biol. Macromol.* <https://doi.org/10.1016/j.ijbiomac.2021.01.210>.
- Mansouri, R., Jouan, Y., Hay, E., Blin-Wakkach, C., Frain, M., Ostertag, A., Henaff, C.L., Marty, C., Geoffroy, V., Marie, P.J., Cohen-Solal, M., Modrowski, D., 2017. Osteoblastic heparan sulfate glycosaminoglycans control bone remodeling by regulating Wnt signaling and the crosstalk between bone surface and marrow cells. *Cell Death Dis.* <https://doi.org/10.1038/CDDIS.2017.287>.
- Murali, S., Kumar, S., Koh, J., Seenaa, S., Singh, P., Ramalho, A., Sobral, A.J.F.N., 2019. Bio-based chitosan/gelatin/Ag@ZnO bio-nanocomposites: synthesis and mechanical and antibacterial properties. *Cellulose.* <https://doi.org/10.1007/s10570-019-02457-2>.
- Nikpour, M.R., Rabiee, S.M., Jahanshahi, M., 2012. Synthesis and characterization of hydroxyapatite/chitosan nanocomposite materials for medical engineering applications. *Compos. Part B Eng.* <https://doi.org/10.1016/j.compositesb.2012.01.056>.
- Nosrati, H., Mamoori, R.S., Le, D.Q.S., Bünger, C.E., 2019. Preparation of reduced graphene oxide/hydroxyapatite nanocomposite and evaluation of graphene sheets/hydroxyapatite interface. *Diam. Relat. Mater.* <https://doi.org/10.1016/j.diamond.2019.107561>.
- Panda, N.R., Acharya, B.S., Nayak, P., Bag, B.P., 2014. Studies on growth morphology, UV absorbance and luminescence properties of sulphur doped ZnO nanopowders synthesized by the application of ultrasound with varying input power. *Ultrason. Sonochem.* <https://doi.org/10.1016/j.ultsonch.2013.08.007>.
- Pereira, I.C., Duarte, A.S., Neto, A.S., Ferreira, J.M.F., 2019. Chitosan and polyethylene glycol based membranes with antibacterial properties for tissue regeneration. *Mater. Sci. Eng. C.* <https://doi.org/10.1016/j.msec.2018.11.029>.
- Rahman, M.A., Islam, M.S., Haque, P., Khan, M.N., Takafuji, M., Begum, M., Chowdhury, G.W., Khan, M., Rahman, M.M., 2020. Calcium ion mediated rapid wound healing by nano-ZnO doped calcium phosphate-chitosan-alginate biocomposites. *Materialia.* <https://doi.org/10.1016/j.mtla.2020.100839>.
- Ratha, I., Datta, P., Balla, V.K., Nandi, S.K., Kundu, B., 2021. Effect of doping in hydroxyapatite as coating material on biomedical implants by plasma spraying method: a review. *Ceram. Int.* <https://doi.org/10.1016/j.ceramint.2020.10.112>.
- Ressler, A., Žužić, A., Ivanišević, I., Kamboj, N., Ivanković, H., 2021. Ionic substituted hydroxyapatite for bone regeneration applications: a review. *Open Ceram.* <https://doi.org/10.1016/j.oceram.2021.100122>.
- Ressler, A., Antunović, M., Teruel-Biosca, L., Ferrer, G.G., Babić, S., Urlić, I., Ivanković, M., Ivanković, H., 2022a. Osteogenic differentiation of human mesenchymal stem cells on substituted calcium phosphate/chitosan composite scaffold. *Carbohydr. Polym.* <https://doi.org/10.1016/j.carbpol.2021.118883>.
- Ressler, A., Kamboj, N., Ledinski, M., Rogina, A., Urlić, I., Hussainova, I., Ivanković, H., Ivanković, M., 2022b. Macroporous silicon-wollastonite scaffold with Sr/Se/Zn/Mg-substituted hydroxyapatite/chitosan hydrogel. *Open Ceram.* 12, 1–9. <https://doi.org/10.1016/j.oceram.2022.100306>.
- Rong, P., Ren, S., Yu, Q., 2019. Fabrications and applications of ZnO nanomaterials in flexible functional devices-a review. *Crit. Rev. Anal. Chem.* <https://doi.org/10.1080/10408347.2018.1531691>.
- Roseti, L., Parisi, V., Petretta, M., Cavallo, C., Desando, G., Bartolotti, I., Grigolo, B., 2017. Scaffolds for bone tissue engineering: state of the art and new perspectives. *Mater. Sci. Eng. C.* <https://doi.org/10.1016/j.msec.2017.05.017>.
- Sani, I.K., Pirsaa, S., Tađi, Š., 2019. Preparation of chitosan/zinc oxide/Melissa officinalis essential oil nano-composite film and evaluation of physical, mechanical and antimicrobial properties by response surface method. *Polym. Test.* <https://doi.org/10.1016/j.polymertesting.2019.106004>.
- Sarma, G.K., Sharma, R., Saikia, R., Borgohain, X., Iraqui, S., Bhattacharyya, K.G., Rashid, M.H., 2020. Facile synthesis of chitosan-modified ZnO/ZnFe2O4 nanocomposites for effective remediation of groundwater fluoride. *Environ. Sci. Pollut. Res.* <https://doi.org/10.1007/s11356-020-09270-6>.
- Tan, H., Chu, C.R., Payne, K.A., Marra, K.G., 2009. Injectable in situ forming biodegradable chitosan-hyaluronic acid based hydrogels for cartilage tissue engineering. *Biomaterials.* <https://doi.org/10.1016/j.biomaterials.2008.12.080>.
- Tantiwatcharothai, S., Prachayawarakorn, J., 2019. Characterization of an antibacterial wound dressing from basil seed (Ocimum basilicum L.) mucilage-ZnO nanocomposite. *Int. J. Biol. Macromol.* <https://doi.org/10.1016/j.ijbiomac.2019.05.118>.
- Thomas, M.S., Koshy, R.R., Mary, S.K., Thomas, S., A. Pothan, L., 2019. Starch, Chitin and Chitosan Based Composites and Nanocomposites, Springer Brieds in Molecular Science Biobased Polymers. ISBN: 978-3-030-03158-9.
- Warastuti, Y., Budianto, E., Darmawan, D., 2018. Sintesis dan Karakterisasi Membran Komposit Hidroksiapatit Tulang Sapi-Khitosan-Poli(Vinilalkohol) untuk Aplikasi Biomaterial. *Jusami | Indones. J. Mater. Sci.* <https://doi.org/10.17146/jsmi.2015.16.2.4021>.
- Wicaksono, S.T., Rasyida, A., Purnomo, A., Pradita, N.N., Ardhyanaanta, H., Hidayat, M.I.P., 2017. Composite Based Chitosan/Zinc-Doped HA as a Candidate Material for Bone Substitute Applications, in: IOP Conference Series: Materials Science and Engineering. <https://doi.org/10.1088/1757-899X/202/1/012080>.
- Yigit, O., Dikici, B., Kaseem, M., Nakai, M., Niinomi, M., 2022. Facile formation with HA/Sr-GO-based composite coatings via green hydrothermal treatment on β -type TiNbTaZr alloys: Morphological and electrochemical insights. *J. Mater. Res.* <https://doi.org/10.1557/s43578-021-00470-5>.
- Yigit, O., Dikici, B., Senocak, T.C., Ozdemir, N., 2020. One-step synthesis of nano-hydroxyapatite/graphene nanosheet hybrid coatings on Ti6Al4V alloys by hydrothermal method and their in-vitro corrosion responses. *Surf. Coatings Technol.* <https://doi.org/10.1016/j.surfcoat.2020.125858>.